DOI 10.1515/hsz-2013-0165 — Biol. Chem. 2013; 394(11): 1357–1370

Review

Ananda Ayyappan Jaguva Vasudevan, Sander H.J. Smits, Astrid Höppner, Dieter Häussinger, Bernd W. Koenig and Carsten Münk*

Structural features of antiviral DNA cytidine deaminases

Abstract: The APOBEC3 (A3) family of cytidine deaminases plays a vital role for innate defense against retroviruses. Lentiviruses such as HIV-1 evolved the Vif protein that triggers A3 protein degradation. There are seven A3 proteins, A3A-A3H, found in humans. All A3 proteins can deaminate cytidines to uridines in single-stranded DNA (ssDNA), generated during viral reverse transcription. A3 proteins have either one or two cytidine deaminase domains (CD). The CDs coordinate a zinc ion, and their amino acid specificity classifies the A3s into A3Z1, A3Z2, and A3Z3. A3 proteins occur as monomers, dimers, and large oligomeric complexes. Studies on the nature of A3 oligomerization, as well as the mode of interaction of A3s with RNA and ssDNA are partially controversial. High-resolution structures of the catalytic CD2 of A3G and A3F as well as of the single CD proteins A3A and A3C have been published recently. The NMR and X-ray crystal structures show globular proteins with six α-helices and five β sheets arranged in a characteristic motif (α1-β1-β2/2′-α2-β3-α3-β4-α4-β5-α5-α6). However, the detailed arrangement and extension of individual structure elements and their relevance for A3 complex formation and activity remains a matter of debate and will be highlighted in this review.

Keywords: APOBEC3G; HIV-1; homology modeling; NMR; Vif; X-ray.

***Corresponding author: Carsten Münk,** Clinic for Gastroenterology, Hepatology, and Infectiology, Medical Faculty, Heinrich-Heine-University, D-40225 Düsseldorf, Germany,
e-mail: carsten.muenk@med.uni-duesseldorf.de
Ananda Ayyappan Jaguva Vasudevan and Dieter Häussinger: Clinic for Gastroenterology, Hepatology, and Infectiology, Medical Faculty, Heinrich-Heine-University, D-40225 Düsseldorf, Germany
Sander H.J. Smits: Institute of Biochemistry, Heinrich-Heine-University, D-40225 Düsseldorf, Germany
Astrid Höppner: Crystal and X-Ray Facility, Heinrich-Heine-University, D-40225 Düsseldorf, Germany
Bernd W. Koenig: Institute of Structural Biochemistry (ICS-6), Research Centre Jülich, D-52425 Jülich, Germany

Introduction: APOBEC3s – mammal-specific antiviral polynucleotide cytidine deaminases with oncogenic potential

Apolipoprotein B mRNA editing enzyme, catalytic polypeptide-like (APOBEC3, A3) genes are found only in placental mammals, but might be evolutionary, as old as the origin of mammals (LaRue et al., 2008; Münk et al., 2012b). All seven human A3 proteins (A3A, A3B, A3C, A3D, A3F, A3G, and A3H, Figure 1A) are single-strand DNA (ssDNA) cytidine deaminases known to inhibit multiple retroviruses, retroelements, RNA and DNA viruses (Arias et al., 2012). Many important aspects of the biology of A3 proteins are not resolved, and it is still unknown how A3s discern self from non-self ssDNA. Recent data support a role of human A3 proteins, especially for A3B, to act oncogenic and cause C-to-T mutations in breast cancer tissue (Nik-Zainal et al., 2012; Roberts et al., 2012; Burns et al., 2013; Nowarski and Kotler, 2013; Taylor et al., 2013).

The deaminases possess either one or two conserved zinc-coordinating (Z) motifs, in which the zinc is coordinated by a histidine and two cysteines. Z motifs can be classified into three groups (Z1, Z2, Z3), but share the consensus amino acid signature H-X-E-X_{24-31}C-X_{2-4}C (where X can be nearly any residue) (Jarmuz et al., 2002; Conticello, 2008; LaRue et al., 2008, 2009; Münk et al., 2008, 2012b) (Figure 1B).

A3G, the best-studied A3 protein (Harris et al., 2002; Jarmuz et al., 2002), is an inhibitor of variants of HIV-1 lacking the Vif gene expression (HIV-1ΔVif) in peripheral blood mononuclear cells (Sheehy et al., 2002). During retroviral budding, A3G binds to the viral nucleocapsid protein, can be incorporated into HIV-1ΔVif progeny particles, and carried over within the virion. In the virion, A3G proteins are then processed and cleansed of an inhibitory RNA by the viral RNase H (Soros et al., 2007). After cell entry, the viral genomic (+) strand RNA is reverse

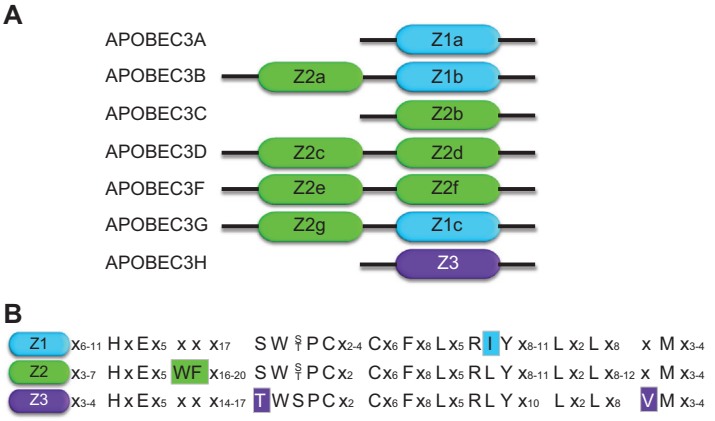

Figure 1 Human APOBEC3 proteins.
(A) Schematic representation of human APOBEC3 (A3) cytidine deaminases. All A3 proteins share at least one zinc (Z)-coordinating catalytic motif. The color code indicates the amino acid specificity of the different Z-motif-containing deaminase domains (Z1, Z2, and Z3). In humans, seven A3 proteins are detectable, A3A-A3H. (B) Amino acid sequences of indicated domains. Group-specific distinctions of Z-domains are highlighted.

transcribed into the (-) strand DNA that is the template for the (+) strand DNA synthesis, generating a complete, double-stranded viral DNA. Particle-delivered A3G proteins can inhibit HIV through multiple mechanisms early in the infection cycle, by cytidine deamination of the ssDNA and by reducing the reverse transcription and integration (for recent reviews, see Albin and Harris, 2010; Wissing et al., 2010; Münk et al., 2012a). In the virus-producer cell, Vif binding to A3G will induce polyubiquitylation and degradation of A3G, resulting in A3G-free progeny virions. To achieve polyubiquitylation and subsequent degradation of A3G, Vif acts as an A3G substrate receptor molecule by mimicking the SOCS-box component of a cellular E3 ubiquitin ligase in the Vif-Cullin5-Elongin B/C ubiquitin ligase complex (Marin et al., 2003; Sheehy et al., 2003; Yu et al., 2003, 2004; Mehle et al., 2004; Bergeron et al., 2010). Vif additionally recruits the transcription cofactor CBF-β to form this active complex (Jager et al., 2012; Zhang et al., 2012). The A3-Vif interaction is critical: Vif efficiently, but not completely, counteracts A3C, A3D, A3F, A3G, and A3H. A3 proteins that do not bind to Vif are not neutralized and likely inhibit HIV (for a review, see Münk et al., 2012a). A3 antagonists that presumably play a similar role as Vif proteins of lentiviruses have been described for other viruses, too: the Bet proteins in foamy retroviruses, the nucleocapsid protein in human T-cell lymphotropic virus type 1, and the glycosylated Gag protein (glyco-Gag) of murine leukemia virus have been implicated in the counteraction of the antiviral activity of A3 proteins (Mariani et al., 2003; Löchelt et al., 2005; Russell et al., 2005; Derse et al., 2007; Münk et al., 2008; Perkovic et al., 2009; Kolokithas et al., 2010; Chareza et al., 2012; Ooms et al., 2012; Jaguva Vasudevan et al., 2013; Stavrou et al., 2013).

A3G is a two-domain deaminase with a Z2 and a Z1 domain (Z2g-Z1c, Figure 1B). These two functionally distinct subunits, the N-terminal pseudocatalytic domain (CD1, residues 1–196), which is more positively charged under physiological conditions, and the C-terminal catalytic domain (CD2, residues 197–384) give the protein an internal pseudosymmetry (Huthoff et al., 2009; Chelico et al., 2010; Feng and Chelico, 2011). Genetic and biochemical data illustrate that the CD2 in the context of the full-length A3G alone is responsible for the deamination activity, whereas the CD1 is more important for binding of RNA or ssDNA (Hache et al., 2005; Navarro et al., 2005; Schumacher et al., 2008; Huthoff et al., 2009; Chelico et al., 2010; Feng and Chelico, 2011). After binding randomly to ssDNA, but not to double-stranded DNA (dsDNA), A3G translocates arbitrarily in small steps by sliding along the polynucleotide and in larger steps by jumping/hopping or intersegmental transfer (Chelico et al., 2006, 2008; Nowarski et al., 2008; Shlyakhtenko et al., 2011, 2012). The deamination in the CCC motif occurs processively, i.e., one A3G molecule catalyses multiple deaminations on the same ssDNA prior to attacking a different substrate (Chelico et al., 2006, 2008). In the A3G recognition motif, the pyrimidine rings of the -2 and -1 cytidine residues are essential for motif recognition and deamination of the third (0) cytidine residue (Rausch et al., 2009). Several studies indicate that A3G deaminates predominantly in the 3′-to-5′ direction, where the CD1 domain is probably required for introducing this bias (Chelico et al., 2006, 2008, 2010; Holden et al., 2008; Furukawa et al., 2009).

Oligomeric organization of APOBEC3s

What is the preferred oligomerization state of A3G and other A3 proteins in human cells? Does the cytidine deamination activity or the antiviral function of A3s require monomers, dimers, or higher-order oligomers? Questions like this have been addressed by many investigations using several different techniques.

A3G and A3F isolated by gel filtration chromatography from human or baculovirus-infected Sf9 cells revealed protein complexes of >700 kDa, implicating either homomultimerization of A3s and/or interactions with additional protein species (Chelico et al., 2006; Chiu et al., 2006; Kozak et al., 2006; Kreisberg et al., 2006). Studies also described dimerization and higher-order oligomers of A3B and A3C in living cells as well as *in vitro* (Chiu et al., 2006; Wedekind et al., 2006; Niewiadomska et al., 2007; Chen et al., 2008; Holden et al., 2008; Wang et al., 2008; Huthoff et al., 2009; Salter et al., 2009; Stauch et al., 2009; Chelico et al., 2010; Shandilya et al., 2010).

A3G can exist as monomers, dimers, or megadalton oligomers, the so-called high molecular mass (HMM) complexes (Jarmuz et al., 2002; Chiu et al., 2006; Wedekind et al., 2006; Bennett et al., 2008). Resting CD4 T cells and monocytes show low molecular mass (LMM) A3G complexes, and activation of CD4 T cells promotes the recruitment of LMM A3G and subsequent formation of HMM complexes (Kreisberg et al., 2006). A3G has RNA-binding properties (Jarmuz et al., 2002; Iwatani et al., 2006; Kozak et al., 2006; Huthoff et al., 2009). RNA digestion in cell lysates initially containing HMM complexes resulted in LMM complexes supporting the notion that HMM complexes are ribonucleoprotein complexes (Kreisberg et al., 2006). Using tandem affinity purification techniques coupled with mass spectrometry, specific components of the HMM A3G and A3F complexes were identified to bind RNA like in Staufen-containing RNA-transporting granules and in Ro ribonucleoprotein complexes (Chiu et al., 2006), poly(A)-binding proteins (Kozak et al., 2006), in P bodies (Gallois-Montbrun et al., 2007, 2008), and in stress granules (Kozak et al., 2006; Gallois-Montbrun et al., 2007, 2008). Analysis of RNAs in these complexes revealed HIV-1 RNA, Alu, small Y RNAs, certain mRNAs (such as that encoding A3G itself), and the 7SL RNA of the signal recognition particle (Chiu et al., 2006; Kozak et al., 2006; Gallois-Montbrun et al., 2008).

To obtain structural models of the A3G HMM or LMM complexes, small-angle X-ray scattering (SAXS) was applied to Sf9 cell-derived A3G (Wedekind et al., 2006). Low-resolution molecular envelopes were derived from the SAXS data. RNase A treatment of the samples resulted in an SAXS profile consistent with an A3G dimer. The SAXS-derived molecular envelope of the untreated A3G was significantly larger and could accommodate two A3G dimer envelopes with no spatial overlap (Wedekind et al., 2006). The authors described the shape of the RNA-containing A3G oligomer, which likely presents a minimal HMM particle, as an elongated cylinder, formed by two A3G dimers. These two A3G dimers appear to associate in a tail-to-tail fashion (protein-protein interactions via the C termini) rather than in a head-to-head or head-to-tail configuration. In contrast, cross-linking experiments showed A3G dimers that appear to be arranged in a head-to-head fashion with the two N-terminal CD1 domains forming the contact. Mutating the CD1 of A3G abrogates its RNA binding and self-association potential (Navarro et al., 2005; Friew et al., 2009). Specifically, the conserved W94, Y124, and W127 within the CD1 domain mediate A3G oligomerization and packaging into HIV-1 virions (Bulliard et al., 2009; Huthoff et al., 2009). Oligomerization-deficient A3G proteins associate less efficiently with several cellular RNA molecules, supporting a model that occupation of the positively charged pocket by RNA promotes A3G oligomerization (Bulliard et al., 2009; Huthoff et al., 2009). Because native A3G can form oligomers larger than dimers, an additional oligomer interface apart from CD1-CD1 is likely to exist (Chelico et al., 2010).

The oligomerization state of A3G was analyzed by multiangle light scattering (MALS) (Chelico et al., 2010). Purified A3G is a polydisperse mixture, primarily containing dimers (~80%), along with subpopulations of monomers (~18%), and higher-order oligomers (~2%). These findings are in agreement with analytical ultracentrifugation data (Salter et al., 2009). A3G is packaged into HIV particles as a multimer, perhaps by interacting with the Alu portion of 7SL RNA or HIV RNA, but presumably not as a monomer (Burnett and Spearman, 2007; Strebel and Khan, 2008). To characterize the oligomerization state of A3G while catalyzing the deamination of HIV proviral cDNA, atomic force microscopy (AFM) was employed to investigate the dynamics and structural determinants of A3G bound to ssDNA (Chelico et al., 2008, 2010; Shlyakhtenko et al., 2011, 2012).

The first reported A3G AFM experiments suggested that A3G forms stable complexes of higher-order oligomers with ssDNA, and the stoichiometry of these complexes depended on salt concentrations and divalent cations (Chelico et al., 2008, 2010). Without salt, the binding of ssDNA appears to cause A3G dissociation from higher-order oligomers to predominantly monomers and dimers

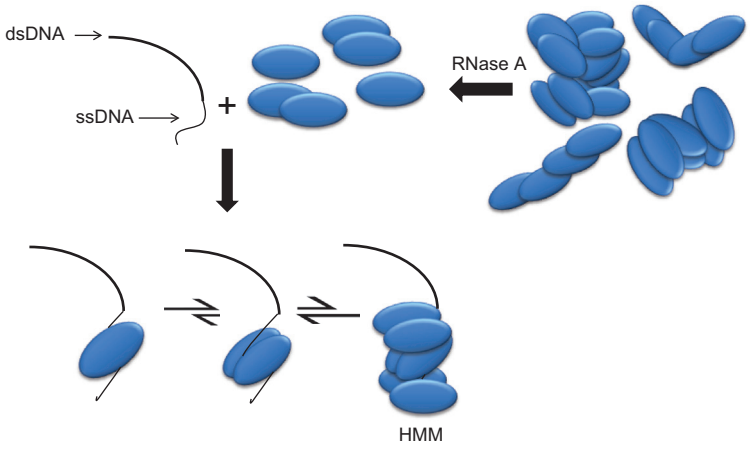

Figure 2 Possible ways of (*in vitro*) A3G-ssDNA interaction studied by AFM.
A hybrid DNA substrate made up of dsDNA (thick) and an ssDNA tail (where A3G binds). One blue oval unit represents a full-length A3G molecule. Free A3G can exist as monomers and dimers (RNase treated). A3G complexed with ssDNA is primarily dimeric, but A3G monomers or higher-order oligomers (HMM; high molecular mass complexes) can also bind ssDNA substrates (adapted from Shlyakhtenko et al., 2011).

(Chelico et al., 2008). Applying an improved hybrid ssDNA substrate Shlyakhtenko et al. demonstrated later that ssDNA-complexed A3G is mostly dimeric, unbound A3G was predominantly monomeric, and A3G monomers, dimers, and higher-order oligomers could bind ssDNA substrates in a manner independent of strand polarity and availability of free ssDNA ends (Shlyakhtenko et al., 2011, 2012). Together, these data suggest that RNA-free A3G oligomerizes upon binding ssDNA substrate, that the dimers form more stable complexes than monomers, and that oligomerization equilibrium is toward dimers (Figure 2).

NMR and crystal structures of APOBEC3s

Three nuclear magnetic resonance (NMR) structures and four X-ray crystal structures of the A3G CD2 catalytic domain have been published to date (Chen et al., 2008; Holden et al., 2008; Furukawa et al., 2009; Harjes et al., 2009; Shandilya et al., 2010; Li et al., 2012). In addition, crystal structures of the A3F CD2 catalytic domain (Bohn et al., 2013) and of A3C were determined (Kitamura et al., 2012). Very recently, the NMR structure of A3A became available (Byeon et al., 2013). However, an experimental structure of the full-length A3G is still missing.

The characteristic architecture of A3G CD2 is a hydrophobic five-stranded core β sheet surrounded by six α-helices, called β1-β5 and α1-α6, respectively, throughout this review. Please note a different numbering scheme in two of the original papers where the N-terminal helix was missing (Chen et al., 2008) or termed α0 (Furukawa et al., 2009). Structures have been determined for variants of different length reflecting the wild type and two CD2 mutants (dubbed A3G-2K3A and A3G-2K2A) of human A3G (see Table 1 for details). In A3G-2K3A, the solubility of the monomeric protein was increased by lysine substitutions L234K and F310K in combination with C243A, C321A, and C356A to minimize the chance of intermolecular disulfide bond formation and to promote long-term stability (Chen et al., 2008). In A3G-2K2A, C321 was not mutated in order to study C321's interaction with the inhibitor compound MN30 (Li et al., 2012). Structure elements in A3G CD2 are arranged in the order of α1-β1-β2/2′-α2-β3-α3-β4-α4-β5-α5-α6 (Figure 3A). The second β strand is divided and forms a β2-bulge-β2′ region (Chen et al., 2008; Furukawa et al., 2009; Harjes et al., 2009; Shandilya et al., 2010). Only one X-ray structure shows a continuous β2 strand (Holden et al., 2008), resembling the distantly related APOBEC2 structure (Prochnow et al., 2007), but this continuous β2 strand in A3G CD2 was heavily disputed and might be an artifact (Harjes et al., 2009; Shandilya et al., 2010). Autore et al. observed a general trend toward the ordered conformations of the β2 strand during molecular dynamics (MD) simulations of the NMR structures, which had a distorted starting conformation of β2 (Autore et al., 2010). This revealed that this distortion is dependent on preferential hydration of residues within the β2 strand, which in turn forms a continuous β sheet in the full length CD1 and CD2 assembly.

Table 1 APOBEC3 and APOBEC2 structures with references.

Subject	Method	PDB code	Protein	Reference
Human APOBEC3G	X-ray crystallography	3E1U/ 3IQS	A3G AA 197-380	(Holden et al., 2008)
		3IR2	A3G AA 191-384 mutation 2K3A[a]	(Shandilya et al., 2010)
		3V4K	A3G AA 191-380 mutation 2K2A[b]	(Li et al., 2012)
		3V4J	A3G AA 191-384 mutation 2K3A[a] MN30 bound	(Li et al., 2012)
	Solution NMR	2JYW	A3G AA 198-384 mutation 2K3A[a]	(Chen et al., 2008)
		2KBO	A3G AA 193-384	(Furukawa et al., 2009)
		2KEM	A3G AA 191-384 mutation 2K3A[a]	(Harjes et al., 2009)
Human APOBEC3F	X-ray crystallography	4IOU	A3F AA 185-373 mutation 11X[c]	(Bohn et al., 2013)
Human APOBEC3A	Solution NMR	2M65	A3A AA 1-199	(Byeon et al., 2013)
Human APOBEC3C	X-ray crystallography	3VOW/ 3VM8	A3C AA 1-190	(Kitamura et al., 2012)
Human APOBEC2	X-ray crystallography	2NYT	A2 AA 41-224	(Prochnow et al., 2007)
Modeled structures	Homology modeling		A3G AA 1-384	(Zhang et al., 2007)
			A3G AA 1-384	(Harjes et al., 2009)
			A3G dimer model	(Bulliard et al., 2009; Huthoff et al., 2009)
			A3C AA 1-190	(Stauch et al., 2009)

[a]2K3A Mutation: L234K, F310K, C243A, C321A, C356A.
[b]2K2A Mutation: L234K, F310K, C243A, C356A.
[c]11X Mutation: Y196D, H247G, C248R, C259A, F302K, W310D, Y314A, Q315A, K355D, K358D, F363D.
MN30, methyl-3,4-dephostatin; AA, amino acid.

The catalytic zinc is coordinated directly by H257, C288, and C291 and indirectly by the catalytic residue E259 via a water molecule (Holden et al., 2008). The zinc-coordinating active site, α2-β3-α3, is anchored within the platform of β strands. The catalytic site is further supported by the α5- and α6-helices, which make extensive stabilizing hydrophobic contacts with the β-strand platform (Chen et al., 2008). Despite the common characteristic fold of the published A3G CD2 structures, they show conformational differences in several functionally important regions.

The first NMR structure of A3G198-384 (2K3A mutant, PDB accession 2JYW) was reported by Chen et al. (2008). Residues 198–384 of A3G were sufficient for DNA deamination. The authors also titrated ^{15}N-labeled A3G-2K3A with a nonlabeled 21-base ssDNA and recorded a series of 2D HSQC NMR spectra of the protein to understand how A3s recognize ssDNA. Resulting changes in NMR signal position (chemical shift perturbation, CSP) or NMR signal intensity indicate binding of the ligand. The strength of the CSP observed for a given amino acid residue is often inversely related to the distance of this residue to the site of binding in the complex. Significant CSPs were detected for the conserved R215 and R313, residues adjacent to R313 within the loop between β4 and α4 (β4-α4 loop) and the catalytic E259 (Chen et al., 2008). These results suggested a DNA-binding model in which a brim of positively charged residues (arginines 213, 215, 313, 320) positions the target cytosine for catalysis that cannot access the catalytic glutamate E259 without flipping out from the phosphodiester backbone (Figure 3B). The presumable orientation of the ssDNA relative to A3G in the complex was deduced from

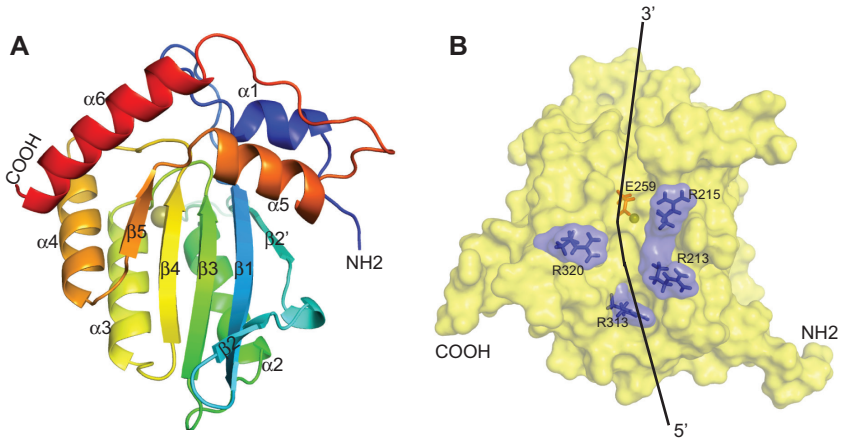

Figure 3 Structure of the CD2 (Z1c) of A3G.
(A) A3G-CD2 structure [PDB 3IR2 (Shandilya et al., 2010)] composed of a core hydrophobic five-stranded β sheets (β1-β5) surrounded by six α helices (α1-α6). The coordinating zinc atom is represented as a sphere. (B) A3G CD2 catalytic domain-DNA interaction model based on the report by Chen et al. (2008). Positively charged residues (arginines) surrounding the active site and the catalytically active E259 are labeled. Hhypothetical DNA binding path and the polarity are shown in black dashed line.

previous deaminase crystal structures (Xiang et al., 1997; Teh et al., 2006; Chen et al., 2008).

The solution structure of wild-type A3G193-384 and the position of a 10-mer ssDNA in the complex were also determined in an independent NMR study (Furukawa et al., 2009) (Figure 4). CSPs were observed for residues in the α1 and β1 loop (N208 and R215), in the β2′-α2 loop (C243, A246, E254, R256, and H257), in α2 (L260, C261, F262, L263, V265, and I266), in β4 (V305 and S306), in the β4-α4 loop (D316 and G319), in β5 (I337), in α5 (D348), and in the α5–α6 loop (V351, D352, and D362). This CSP pattern was similar to the one observed in the above titration of A3G-2K3A with ssDNA (Chen et al., 2008). However, additional CSPs were observed upon ssDNA binding to wild-type A3G193-384 (Furukawa et al., 2009). These data imply that the substrate cytidine is positioned close to catalytic E259, conserved S284-W285-S286, and zinc-coordinating H257. The exact location of the interacting ssDNA is controversial. Three different models of the complex were proposed based on CSP data in the two NMR studies and on the crystal structure of wild-type A3G197-380 (Figure 4B) (Chen et al., 2008; Holden et al., 2008; Furukawa et al., 2009). It is possible that different modes of A3G-ssDNA interactions coexist in solution. Furukawa et al. also observed the deamination reaction of a 10-mer ssDNA carrying a C4, C5, and C6 target sequence by wild-type A3G193-384 in an NMR sample tube in real time in a series of 2D ^{1}H-^{13}C HSQC spectra. Conversion of C6 to U6 was completed within 30 min. Deamination of C5 occurs on a much slower time scale of hours (Furukawa et al., 2009).

Another NMR study on the elongated A3G191-384 carrying the 2K3A mutation demonstrated that several residues within α1 stabilize the catalytic core (Harjes et al., 2009). This NMR data was also used to build a model of the full-length A3G that suggested that the CD1 pseudo-active site and the CD2 catalytic domain are located on different faces of the holoenzyme (Harjes et al., 2009).

Recently, the high-resolution NMR structure of full-length human A3A, the single CD A3Z1a protein, was published (Byeon et al., 2013) (Figure 5). Comparison with other APOBEC structures reveals that the A3A solution structure most closely resembles crystal structures (see below) of A3C (Kitamura et al., 2012) and of the catalytic CD2 of A3G, in particular, of the mutated A3G-2K3A (Shandilya et al., 2010) and A3G-2K2A (Li et al., 2012) variants (Figure 5), while it shows local differences to published NMR solution structures of the A3G CD2 (Byeon et al., 2013). The A3A structure displays an interrupted β2 strand (β2-bulge-β2′) and an N-terminal helix α1. NMR-based analysis of A3A titrations with various ssDNA substrates showed that specific binding of the substrate involves five A3A regions: the active site, the β2′-α2 loop, the β3-α3 loop, the β4-α4 loop, and helix α4. These regions are situated in a localized manner and cluster around the active site in the A3A structure (Byeon et al., 2013), which strongly contrasts the mapping of ssDNA binding to the CD2 of A3G (Chen et al., 2008; Furukawa et al., 2009). In addition, NMR was used to determine binding affinity of A3A for diverse single-stranded oligonucleotides and to follow substrate deamination in real time (Byeon et al., 2013).

The first crystal structure of A3G CD2 (PDB ID: 3E1U, residues 197–380) was reported by Holden et al. (2008). This protein was soluble, but differed to full-length A3G with a 25-fold lower specific deamination activity,

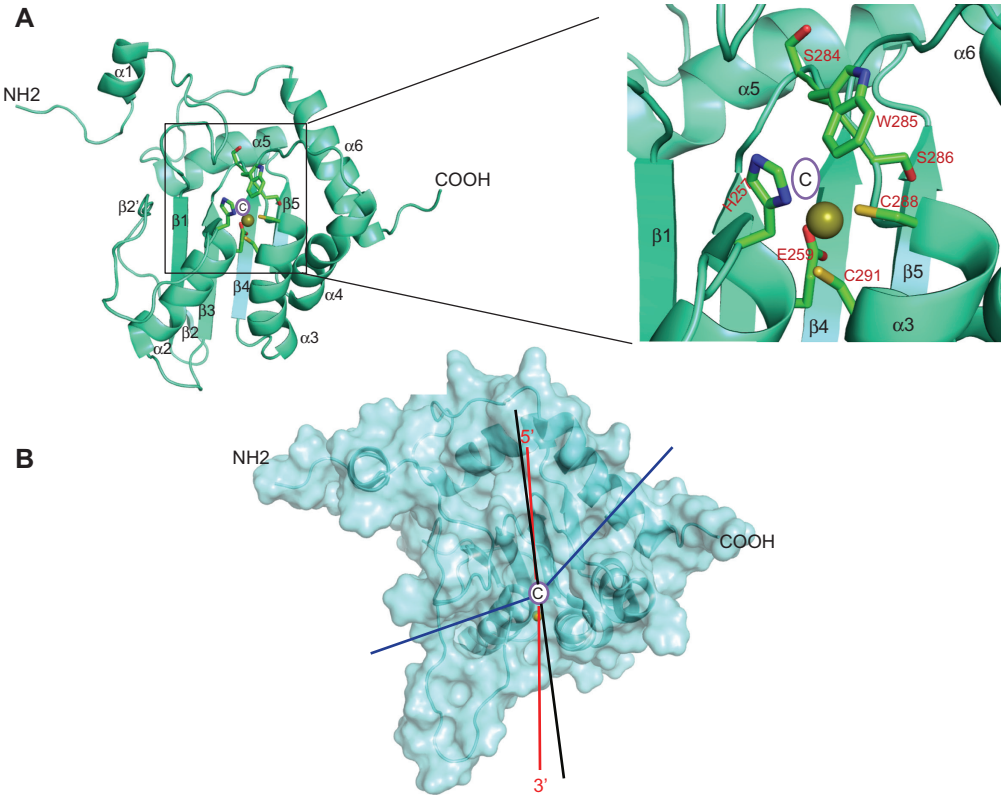

Figure 4 A3G CD2 NMR structure (Furukawa et al., 2009).
(A) Residues close to the zinc-coordinating active center are highlighted in sticks. The possible position of the substrate cytidine is highlighted by an oval shape. (B) Predicted DNA-binding path through the active center of A3G CD2. The broken lines indicate the three different positions of the ssDNA substrate proposed by Chen et al. (2008) (red), Holden et al. (2008) (blue), and Furukawa et al. (2009) (black) are collectively presented.

a twofold reduced processivity, and virtually no 3′ to 5′ deamination bias. The 2.3-Å resolution structure shows a core β sheet that is composed of five β strands surrounded by six α-helices (Holden et al., 2008). In the active site of A3G CD2, a zinc atom is coordinated by the residues H257, C288, and C291, plus a water molecule. In the crystal structure, the CD2 loops 1 and 3 and the regions near the active site form a continuous 'substrate groove' horizontally around the active center. The orientation of this putative substrate groove differs (by 90°) from the groove predicted by the NMR structure (A3G-2K3A) of Chen et al. (2008) (Figure 4B). The groove leads into a deep pocket where the zinc atom is located and continues toward the left side over the α6-helix.

The second crystal structure of A3G CD2 (A3G residue 191-384-2K3A, PDB ID 3IR2) with a resolution of 2.25 Å was presented by Shandilya et al. (2010). This high-resolution crystal structure revealed four extensive protein interfaces (Figure 6A and B), of which one or more may be important

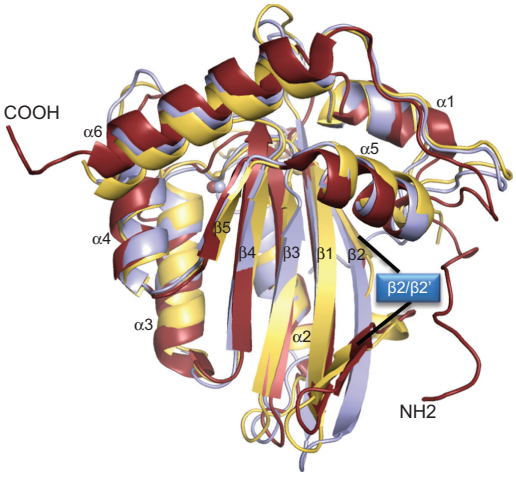

Figure 5 Structure of A3A.
NMR structure of full-length human A3A [ruby, PDB 2M65 (Byeon et al., 2013)] superimposed with the crystal structure of A3G CD2 [yellow, PDB 3IR2 (Shandilya et al., 2010)] and the crystal structure of A3C [light blue; PDB 3VOW; (Kitamura et al., 2012)]. Interrupted β2 sheet of A3A and A3G CD2 is pointed with a dashed line.

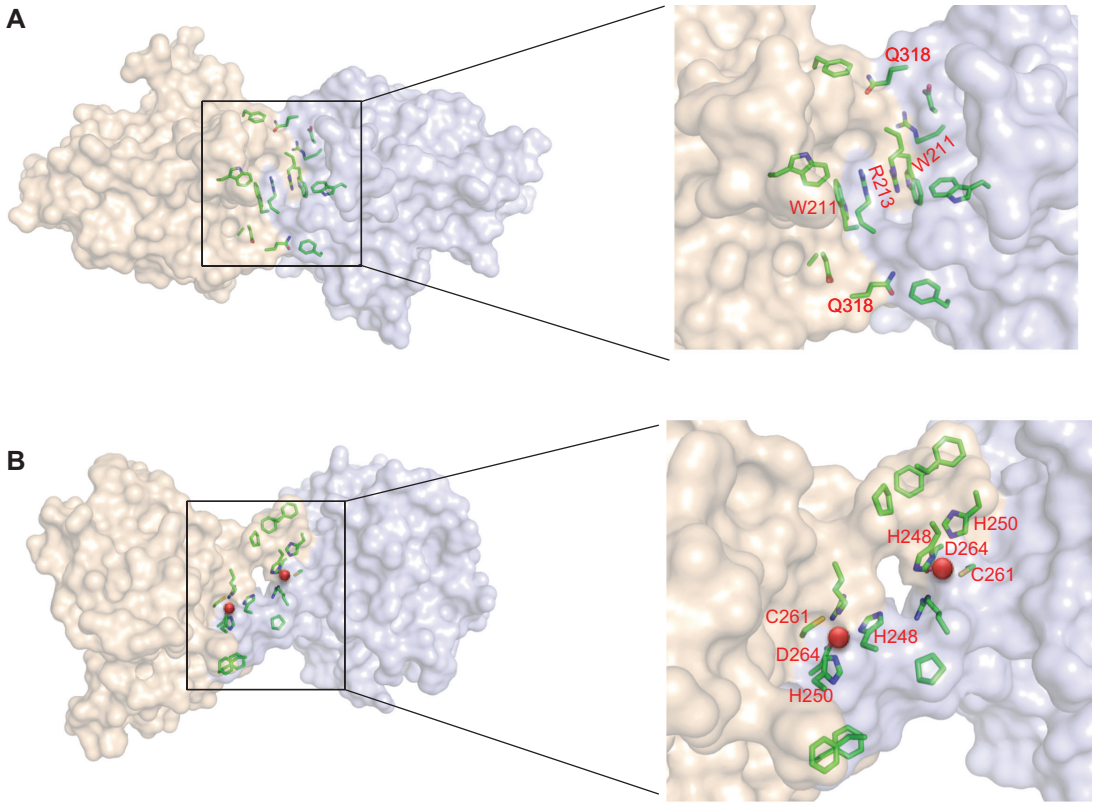

Figure 6 The interfaces of A3G CD2 (PDB 3IR2).
(A) Interface I, the largest interface between two A3G CD2 molecules in the crystal asymmetric unit (computed by PDBePISA). Residues that make this interface are shown in sticks; unique nonconserved residues (W211, R213, Q318) are labeled in red. (B) Interface II, the second largest interface, which coordinates intermolecular zinc (red sphere) through H248 and H250 of one molecule and C261 and D264 (through water-mediated H bond) of the second molecule. The structures were taken from Shandilya et al. (2010).

for A3G oligomerization and HIV restriction activity. The surfaces that form the full-length A3G oligomers remain unclear. SAXS studies have implicated that the C-terminal half of A3G takes part in oligomerization (Wedekind et al., 2006; Bennett et al., 2008). In contrast, coimmunoprecipitation studies demonstrated that N-terminal residues in CD1 are required for RNA-mediated dimerization (Friew et al., 2009; Huthoff et al., 2009). In the A3G CD2 crystal structure (PDB ID 3IR2), the largest interaction interface is determined primarily by contacts between identical residues in the α1-loop-β1 region from both molecules in the asymmetric unit. The second largest interface involves the β2′-loop-α2 residues 247–254 in each of the two molecules of the asymmetric unit. This loop also coordinates an intermolecular zinc-binding site for a second zinc ion, indicating a metal-mediated modulation of A3G oligomerization. The third interface involves residues at N-terminal (β1-β2 strands) and C-terminal ends of A3G-2K3A. The fourth interface is made up of the tops of the α5 and α6 helices (Shandilya et al., 2010). These interaction interfaces observed between molecules in the crystal were explored by the Protein Interfaces, Surfaces and Assemblies Service [PDBePISA (Krissinel and Henrick, 2007)]. It is likely that the residues lining the largest interaction interface (901 Å^2) are essential for both A3G deaminase and antiviral activity and that the second largest interface (604 Å^2) of A3G contributes to its zinc-mediated oligomerization, which may not be essential for A3G's HIV restriction activity. Using NMR, it was further shown that the addition of zinc triggers the oligomer formation, which can be reversed by chelating agents. Based on analyses of the A3G CD2 crystal 3IR2, a variety of potential surfaces could be involved in A3G oligomerization, and a full-length A3G model may give a better understanding about the oligomerization surfaces.

The highest resolution of an A3G CD2 crystal structure (A3G residue 191-384-2K2A, PDB ID 3V4K) published up to now amounts to 1.38 Å and provides full resolution of most amino acid side chains (Li et al., 2012). In the same study, the crystal structure of A3G 191-380-2K3A in complex with the small molecule inhibitor MN30 was solved at 2.04 Å resolution (PDB ID 3V4J). However, the position of the

inhibitor in this crystal structure does most likely not present the primary MN30-binding site in the CD2 of A3G (Li et al., 2012). The authors proposed a model in which the inhibitor molecule MN30 binds specifically to a pocket adjacent to the A3G CD2 active site, reacts covalently with C321, and pushes Y315 into the active site, thereby sterically blocking the entry of substrate DNA cytosines.

The crystal structure of catalytically active and HIV-1 Vif-binding domain of A3F CD2 (A3F residues 185-373-11X, PDB ID 4IOU) was recently solved at 2.75 Å resolution (Bohn et al., 2013). The 11-amino acid-substitution construct rendered enhanced solubility and catalytic activity of the recombinant protein. A3F CD2 has a canonical DNA cytosine deaminase fold, comprised of five β strands and six α helices with the Zn coordination catalytic motif (residues H249, C280, C283, and indirectly by the catalytic residue E251 via a water molecule) (Figure 7). The Zn-coordinating residue C283 and the catalytic residue E251, which are located in helices α2 and α3, define the catalytic pocket. Unlike the disrupted β2 strand of most A3G CD2 structures, A3F CD2 possesses an extended sheet as in A3C and APOBEC2. Despite low sequence similarity, A3F CD2 structure shares the conserved helix (α1 helix) and loop regions with A3G CD2 and A3C (but not with APOBEC2). Four molecules of A3F CD2 build the crystal asymmetric unit. As seen in the A3G CD2 crystal structure (PDB ID 3IR2), A3F structure possessed two unique intermolecular interfaces, but it does not contain the second Zn coordination site as in A3G CD2. The largest isologous interface formed across identical regions of the two chains B and D (Figure 7) and buries a total of 657 Å^2 surface area. The contacts occurred between β1-β2 loop, α2-β3 loop, α3-β4 loop, and α4-β5 loop regions. The second heterologous interface was observed twice (between chains A and B and C and D) in the asymmetric unit and buries a total of 569 Å^2 (Figure 7). It is interesting to note that the β1–β2 loop region involved in the formation of both interfaces (interface 1 and 2) exists in two distinct conformations depending on the interface.

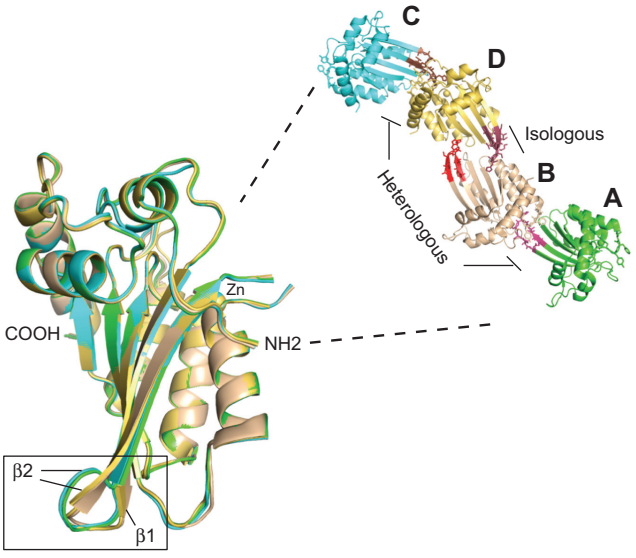

Figure 7 Structure of A3F CD2.
The crystal structure of A3F$_{185\text{-}373}$-11X: A3F CD2 crystal structure asymmetric unit consists of four chains (A, B, C, and D given in green, wheat, yellow, and cyan, respectively). Superimposition of A3F CD2 chains depicts the characteristic fold (five β strands and six α helices) and conformational plasticity in the β1-β2 loop region of the protein (marked with a box). The conserved motif sequence 305-R L Y Y F W D-311 in the β4-α4 loop region involved in heterologous interface colored as the same as the chain color. Isologous interface motifs of β1-β2 loop 223-E V V K H H S P V S-232 in chain A, B, C, D are colored as magenta, red, brown, and raspberry, respectively.

A highly conserved sequence motif across the various human A3s is 305-RLYYFWD-311 in A3F-CTD (β4-α4 loop), which is also conserved across mammalian species infected by lentiviruses. This motif in CD1 and CD2 of A3F is involved in viral encapsidation (Song et al., 2012). In contrast, the less conserved motif of β1-β2 loop region (223-EVVKHHSPVS-232), involved in forming both intermolecular interfaces is not conserved across A3 family members with the exception of A3D-CD2 (Bohn et al., 2013).

The negatively charged molecular surface of A3F CD2 raised some discussion about the Vif A3F interaction (Bohn et al., 2013). It was previously reported that Vif binds to negative surfaces in the α3-α4 helices/the β4 strand and the α2-α3 helices/β3 strand of A3F CD2 (Albin et al., 2010; Smith and Pathak, 2010; Kitamura et al., 2012). This negative surface extends further into the β1-β2 loop region (Bohn et al., 2013). Overall, the negative A3F CD2 surfaces are electrostatically complementary to HIV-1 Vif, a highly basic, intrinsically disordered protein. In addition, BLAST search revealed that both A3F motif sequences (305-RLYYFWD-311 and 223-EVVKHHSPVS-232) align closely with sequences within HIV-1 Vif: 108-HLYYF*D-113 and 23-SLVKHHMYVS-32 (Bohn et al., 2013). This suggests that perhaps HIV-1 Vif evolved to mimic portions of A3F and that the molecular mimicry of Vif could play a role in modulating oligomerization or another molecular recognition event.

The crystal structure of the single CD protein A3C was presented by Kitamura et al. (2012). This structure is of interest because it contains a Vif-binding interface that is absent in A3G CD2, but present in A3G CD1. The full-length A3C protein (residues 1–190) has a core platform composed of six α-helices (α1–α6) and five β strands

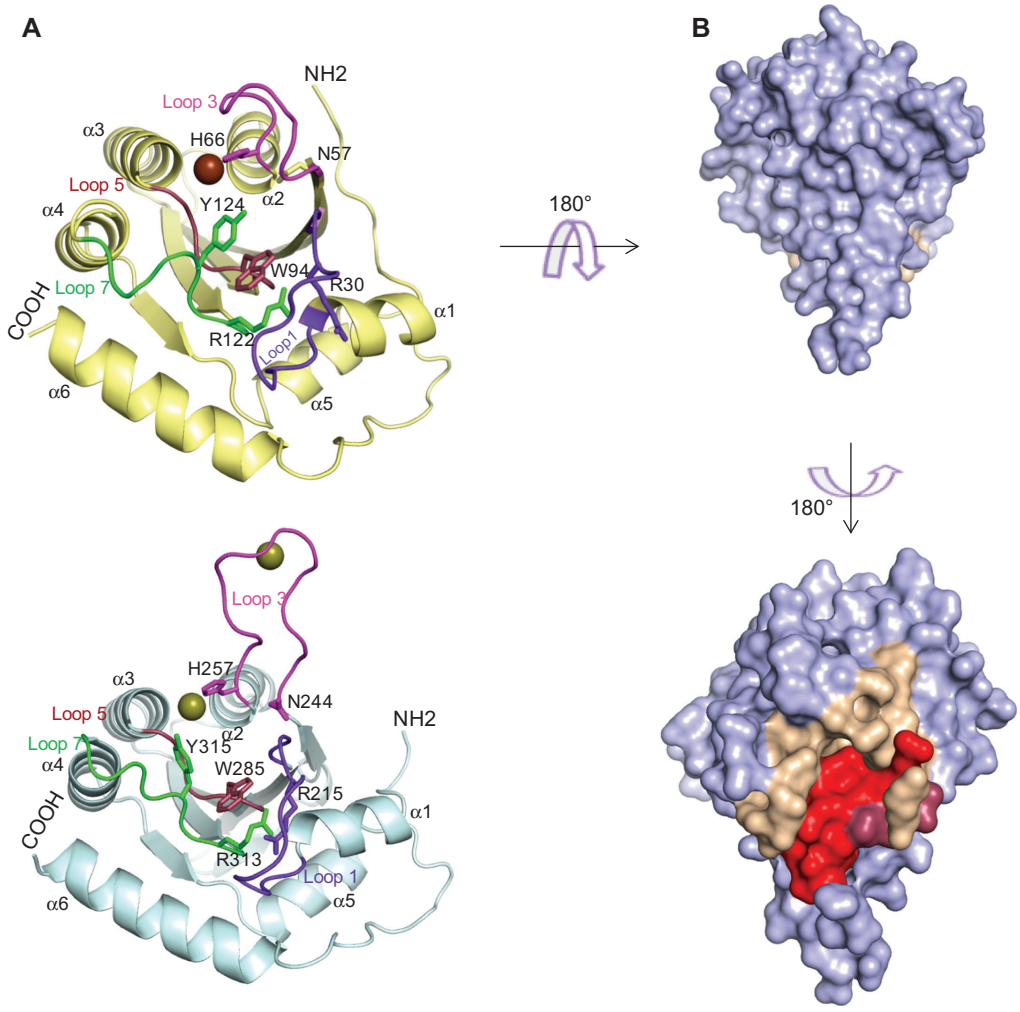

Figure 8 Comparison CD2 of A3G (Z1c) with A3C (Z2b).
(A) Comparison of A3G CD2 (cyan) [PDB 3IR2 (Shandilya et al., 2010)] and A3C (gold) [PDB 3VOW (Kitamura et al., 2012)] crystal structures, conserved amino acids in loop 1 (purple), loop 3 (magenta), loop 5 (brown), and loop 7 (green) are labeled with the residue numbers. (B) HIV-1 Vif-interacting interface on A3C. Structure-guided mutation analysis revealed the critical residues involved in Vif binding. The surface structure depicts the position of the Vif-binding interface on A3C (resides between α2 and α3; shown in wheat), color red (>50% resistance) and raspberry (40–45%) indicates the resistance levels of Vif binding to A3C when they are mutated. Arrows guide to show rotations of the A3C structure.

(β1–β5), with a coordinated zinc ion. Comparing the A3C structure with the structure of A3G CD2 (PDB 3IR2) shows that the core structures are highly conserved, but the loop regions, particularly loops 1, 3, 5, and 7 of the A3C and A3G CD2 structures, are distinct (Figure 8A). The A3C and A3F CD2 structures exhibit a continuous well-ordered β2 strand that is different from the discontinuous β2 strand of the A3G CD2 and the A3A (PDB 2M65). In contrast to the APOBEC2 crystal, where a dimer is formed by pairing two long β2 strands (Prochnow et al., 2007), there were no indications of intermolecular contacts between β2 strands in the A3C crystals (Kitamura et al., 2012). The Vif-binding interface was determined by structure-guided site-directed mutagenesis and revealed the involvement of 10 amino acids for Vif binding located in an area between the α2 and α3 helices, which forms a shallow cavity encompassed by hydrophobic and negatively charged residues (Figure 8B). Additional investigations demonstrated that the Vif-binding interfaces are highly conserved among human Z2-type cytidine deaminases, including A3C, A3F, and A3D, but not A3G (Kitamura et al., 2012).

Coimmunoprecipitation assays with mutants identified by a homology model indicated that aromatic residues F55 and W74 in the respective β2 and α2 region of A3C are important for A3C oligomerization and cytidine deamination activity (Stauch et al., 2009). The core structure of the model A3C was quite similar to that of the experimental crystal structure. The superimposition of model structure

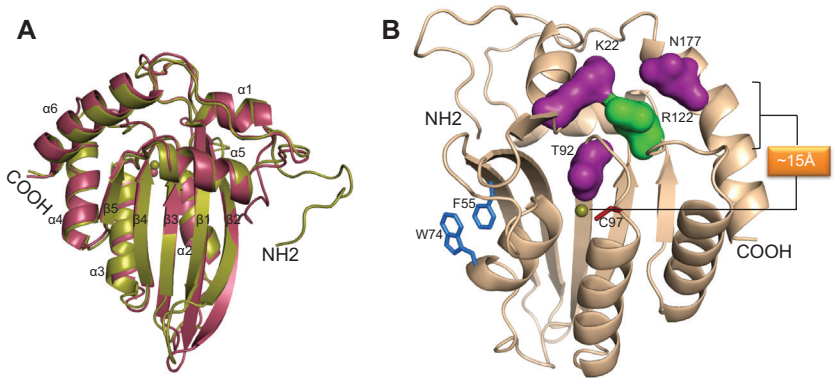

Figure 9 Model structure of A3C.
(A) Superimposition of A3C crystal [PDB 3VOW (Kitamura et al., 2012)] (brown) and model (Stauch et al., 2009) (olive) structures; spheres represent zinc. (B) Model structure of A3C showing the putative substrate-binding pocket (residues shown in surface representation; R122 is colored green), active site amino acid C97 (red) and zinc (sphere), and key dimerization residues (blue sticks).

of A3C core onto the A3C crystal structure (PDB 3VOW) for 98% of the backbone atoms exhibited a Cα root mean square (RMS) deviation of 1.082 Å (187 out of 191 residues) (Figure 9A). R122 in A3C, critical for nucleic acid binding, has essential roles in the efficient RNA-dependent packaging of A3C into virions (Stauch et al., 2009). This residue is involved in the formation of a nucleic acid-binding pocket primarily consisting of loops 1, 3, 5, and 7 of A3C, which is approximately 15 Å distal from the zinc ion coordination site (Figure 9B).

Major challenges

In the last few years, advancements have been made in elucidating the structure of the CD2 catalytic domain of A3G and A3F as well as of A3C and A3A. However, an NMR or crystal structure of the full-length A3G, containing both the CD1 and CD2 domains, is still lacking and urgently needed for defining the biology of this protein. In addition to exploring the structures of all human A3s, there is a need for structures of nonhuman A3, like murine A3 or feline A3s, to describe the structural evolution of these positively selected proteins. Work has to be directed to better understand the regulation of the A3 oligomerization and the interactions with nucleic acids. Co-crystals with ssDNA/RNA and NMR titrations using selected mutants would shed light on the disputed DNA-/RNA-binding regions in A3G. Complex structures of A3s with viral antagonist like Vif or Bet or other viral proteins like the nucleocapsid protein could further expand our understanding of how the rapidly evolving A3s escape recognition by many non-adapted viral antagonists and, at the same time, recognize conserved structures of very diverse viruses. Such knowledge might help to develop new antiretroviral therapeutics that target HIV's interaction with cellular APOBEC3 proteins.

Acknowledgments: We gratefully acknowledge the support (and training) from the International NRW Research School BioStruct, granted by the Ministry of Innovation, Science and Research of the State North Rhine-Westphalia, the Heinrich-Heine-University of Düsseldorf, and the Entrepreneur Foundation at the Heinrich-Heine-University of Düsseldorf. CM is supported by the Heinz Ansmann Foundation for AIDS Research. We thank Lutz Schmitt and Dieter Willbold for their continuous support.

Received April 30, 2013; accepted June 17, 2013; previously published online June 20, 2013

References

Albin, J.S. and Harris, R.S. (2010). Interactions of host APOBEC3 restriction factors with HIV-1 *in vivo*: implications for therapeutics. Expert. Rev. Mol. Med *12*, e4.

Albin, J.S., LaRue, R.S., Weaver, J.A., Brown, W.L., Shindo, K., Harjes, E., Matsuo, H., and Harris, R.S. (2010). A single amino acid in human APOBEC3F alters susceptibility to HIV-1 Vif. J. Biol. Chem. *285*, 40785–40792.

Arias, J.F., Koyama, T., Kinomoto, M., and Tokunaga, K. (2012). Retroelements versus APOBEC3 family members: no great escape from the magnificent seven. Front. Microbiol. *3*, 275.

Autore, F., Bergeron, J.R., Malim, M.H., Fraternali, F., and Huthoff, H. (2010). Rationalisation of the differences between APOBEC3G structures from crystallography and NMR studies by molecular dynamics simulations. PLoS One. *5*, e11515.

Bennett, R.P., Salter, J.D., Liu, X., Wedekind, J.E., and Smith, H.C. (2008). APOBEC3G subunits self-associate via the C-terminal deaminase domain. J. Biol. Chem. *283*, 33329–33336.

Bergeron, J.R., Huthoff, H., Veselkov, D.A., Beavil, R.L., Simpson, P.J., Matthews, S.J., Malim, M.H., and Sanderson, M.R. (2010). The SOCS-box of HIV-1 Vif interacts with ElonginBC by induced-folding to recruit its Cul5-containing ubiquitin ligase complex. PLoS Pathog. *6*, e1000925.

Bohn, M.F., Shandilya, S.M., Albin, J.S., Kouno, T., Anderson, B.D., McDougle, R.M., Carpenter, M.A., Rathore, A., Evans, L., Davis, A.N., et al. (2013). Crystal structure of the DNA cytosine deaminase APOBEC3F: the catalytically active and HIV-1 Vif-binding domain. Structure *21*, 1042–1050.

Bulliard, Y., Turelli, P., Rohrig, U.F., Zoete, V., Mangeat, B., Michielin, O., and Trono, D. (2009). Functional analysis and structural modeling of human APOBEC3G reveal the role of evolutionarily conserved elements in the inhibition of human immunodeficiency virus type 1 infection and Alu transposition. J. Virol. *83*, 12611–12621.

Burnett, A. and Spearman, P. (2007). APOBEC3G multimers are recruited to the plasma membrane for packaging into human immunodeficiency virus type 1 virus-like particles in an RNA-dependent process requiring the NC basic linker. J. Virol. *81*, 5000–5013.

Burns, M.B., Lackey, L., Carpenter, M.A., Rathore, A., Land, A.M., Leonard, B., Refsland, E.W., Kotandeniya, D., Tretyakova, N., Nikas, J.B., et al. (2013). APOBEC3B is an enzymatic source of mutation in breast cancer. Nature *494*, 366–370.

Byeon, I.J., Ahn, J., Mitra, M., Byeon, C.H., Hercik, K., Hritz, J., Charlton, L.M., Levin, J.G., and Gronenborn, A.M. (2013). NMR structure of human restriction factor APOBEC3A reveals substrate binding and enzyme specificity. Nat. Commun. *4*, 1890.

Chareza, S., Slavkovic, L.D., Liu, Y., Rathe, A.M., Münk, C., Zabogli, E., Pistello, M., and Löchelt, M. (2012). Molecular and functional interactions of cat APOBEC3 and feline foamy and immunodeficiency virus proteins: different ways to counteract host-encoded restriction. Virology *424*, 138–146.

Chelico, L., Pham, P., Calabrese, P., and Goodman, M.F. (2006). APOBEC3G DNA deaminase acts processively 3′→5′ on single-stranded DNA. Nat. Struct. Mol. Biol *13*, 392–399.

Chelico, L., Sacho, E.J., Erie, D.A., and Goodman, M.F. (2008). A model for oligomeric regulation of APOBEC3G cytosine deaminase-dependent restriction of HIV. J. Biol. Chem. *283*, 13780–13791.

Chelico, L., Prochnow, C., Erie, D.A., Chen, X.S., and Goodman, M.F. (2010). Structural model for deoxycytidine deamination mechanisms of the HIV-1 inactivation enzyme APOBEC3G. J. Biol. Chem. *285*, 16195–16205.

Chen, K.M., Harjes, E., Gross, P.J., Fahmy, A., Lu, Y., Shindo, K., Harris, R.S., and Matsuo, H. (2008). Structure of the DNA deaminase domain of the HIV-1 restriction factor APOBEC3G. Nature *452*, 116–119.

Chiu, Y.L., Witkowska, H.E., Hall, S.C., Santiago, M., Soros, V.B., Esnault, C., Heidmann, T., and Greene, W.C. (2006). High-molecular-mass APOBEC3G complexes restrict Alu retrotransposition. Proc. Natl. Acad. Sci. USA *103*, 15588–15593.

Conticello, S.G. (2008). The AID/APOBEC family of nucleic acid mutators. Genome Biol. *9*, 229.

Derse, D., Hill, S.A., Princler, G., Lloyd, P., and Heidecker, G. (2007). Resistance of human T cell leukemia virus type 1 to APOBEC3G restriction is mediated by elements in nucleocapsid. Proc. Natl. Acad. Sci. USA *104*, 2915–2920.

Feng, Y. and Chelico, L. (2011). Intensity of deoxycytidine deamination of HIV-1 proviral DNA by the retroviral restriction factor APOBEC3G is mediated by the noncatalytic domain. J. Biol. Chem. *286*, 11415–11426.

Friew, Y.N., Boyko, V., Hu, W.S., and Pathak, V.K. (2009). Intracellular interactions between APOBEC3G, RNA, and HIV-1 Gag: APOBEC3G multimerization is dependent on its association with RNA. Retrovirology *6*, 56.

Furukawa, A., Nagata, T., Matsugami, A., Habu, Y., Sugiyama, R., Hayashi, F., Kobayashi, N., Yokoyama, S., Takaku, H., and Katahira, M. (2009). Structure, interaction and real-time monitoring of the enzymatic reaction of wild-type APOBEC3G. EMBO J. *28*, 440–451.

Gallois-Montbrun, S., Kramer, B., Swanson, C.M., Byers, H., Lynham, S., Ward, M., and Malim, M.H. (2007). Antiviral protein APOBEC3G localizes to ribonucleoprotein complexes found in P bodies and stress granules. J. Virol. *81*, 2165–2178.

Gallois-Montbrun, S., Holmes, R.K., Swanson, C.M., Fernandez-Ocana, M., Byers, H.L., Ward, M.A., and Malim, M.H. (2008). Comparison of cellular ribonucleoprotein complexes associated with the APOBEC3F and APOBEC3G antiviral proteins. J. Virol. *82*, 5636–5642.

Hache, G., Liddament, M.T., and Harris, R.S. (2005). The retroviral hypermutation specificity of APOBEC3F and APOBEC3G is governed by the C-terminal DNA cytosine deaminase domain. J. Biol. Chem. *280*, 10920–10924.

Harjes, E., Gross, P.J., Chen, K.M., Lu, Y., Shindo, K., Nowarski, R., Gross, J.D., Kotler, M., Harris, R.S., and Matsuo, H. (2009). An extended structure of the APOBEC3G catalytic domain suggests a unique holoenzyme model. J. Mol. Biol *389*, 819–832.

Harris, R.S., Petersen-Mahrt, S.K., and Neuberger, M.S. (2002). RNA editing enzyme APOBEC1 and some of its homologs can act as DNA mutators. Mol. Cell *10*, 1247–1253.

Holden, L.G., Prochnow, C., Chang, Y.P., Bransteitter, R., Chelico, L., Sen, U., Stevens, R.C., Goodman, M.F., and Chen, X.S. (2008). Crystal structure of the anti-viral APOBEC3G catalytic domain and functional implications. Nature *456*, 121–124.

Huthoff, H., Autore, F., Gallois-Montbrun, S., Fraternali, F., and Malim, M.H. (2009). RNA-dependent oligomerization of APOBEC3G is required for restriction of HIV-1. PLoS Pathog. *5*, e1000330.

Iwatani, Y., Takeuchi, H., Strebel, K., and Levin, J.G. (2006). Biochemical activities of highly purified, catalytically active human APOBEC3G: correlation with antiviral effect. J. Virol. *80*, 5992–6002.

Jager, S., Kim, D.Y., Hultquist, J.F., Shindo, K., LaRue, R.S., Kwon, E., Li, M., Anderson, B.D., Yen, L., Stanley, D., et al. (2012). Vif hijacks CBF-β to degrade APOBEC3G and promote HIV-1 infection. Nature *481*, 371–375.

Jaguva Vasudevan, A.A., Perkovic, M., Bulliard, Y., Cichutek, K., Trono, D., Haussinger, D., and Munk, C. (2013). Prototype foamy virus bet impairs the dimerization and cytosolic solubility of human APOBEC3G. J. Virol. 2013 Jun 12. [Epub ahead of print].

Jarmuz, A., Chester, A., Bayliss, J., Gisbourne, J., Dunham, I., Scott, J., and Navaratnam, N. (2002). An anthropoid-specific locus of orphan C to U RNA-editing enzymes on chromosome 22. Genomics *79*, 285–296.

Kitamura, S., Ode, H., Nakashima, M., Imahashi, M., Naganawa, Y., Kurosawa, T., Yokomaku, Y., Yamane, T., Watanabe, N., Suzuki, A., et al. (2012). The APOBEC3C crystal structure and the interface for HIV-1 Vif binding. Nat. Struct. Mol. Biol *19*, 1005–1010.

Kolokithas, A., Rosenke, K., Malik, F., Hendrick, D., Swanson, L., Santiago, M.L., Portis, J.L., Hasenkrug, K.J., and Evans, L.H. (2010). The glycosylated Gag protein of a murine leukemia virus inhibits the antiretroviral function of APOBEC3. J. Virol. *84*, 10933–10936.

Kozak, S.L., Marin, M., Rose, K.M., Bystrom, C., and Kabat, D. (2006). The anti-HIV-1 editing enzyme APOBEC3G binds HIV-1 RNA and messenger RNAs that shuttle between polysomes and stress granules. J. Biol. Chem. *281*, 29105–29119.

Kreisberg, J.F., Yonemoto, W., and Greene, W.C. (2006). Endogenous factors enhance HIV infection of tissue naive CD4 T cells by stimulating high molecular mass APOBEC3G complex formation. J. Exp. Med. *203*, 865–870.

Krissinel, E. and Henrick, K. (2007). Inference of macromolecular assemblies from crystalline state. J. Mol. Biol. *372*, 774–797.

LaRue, R.S., Jonsson, S.R., Silverstein, K.A., Lajoie, M., Bertrand, D., El-Mabrouk, N., Hotzel, I., Andresdottir, V., Smith, T.P., and Harris, R.S. (2008). The artiodactyl APOBEC3 innate immune repertoire shows evidence for a multi-functional domain organization that existed in the ancestor of placental mammals. Mol. Biol. *9*, 104.

LaRue, R.S., Andresdottir, V., Blanchard, Y., Conticello, S.G., Derse, D., Emerman, M., Greene, W.C., Jonsson, S.R., Landau, N.R., Löchelt, M., et al. (2009). Guidelines for naming nonprimate APOBEC3 genes and proteins. J. Virol. *83*, 494–497.

Li, M., Shandilya, S.M., Carpenter, M.A., Rathore, A., Brown, W.L., Perkins, A.L., Harki, D.A., Solberg, J., Hook, D.J., Pandey, K.K., et al. (2012). First-in-class small molecule inhibitors of the single-strand DNA cytosine deaminase APOBEC3G. ACS Chem. Biol. *7*, 506–517.

Löchelt, M., Romen, F., Bastone, P., Muckenfuss, H., Kirchner, N., Kim, Y.B., Truyen, U., Rosler, U., Battenberg, M., Saib, A., et al. (2005). The antiretroviral activity of APOBEC3 is inhibited by the foamy virus accessory Bet protein. Proc. Natl. Acad. Sci. USA *102*, 7982–7987.

Mariani, R., Chen, D., Schröfelbauer, B., Navarro, F., König, R., Bollman, B., Münk, C., Nymark-McMahon, H., and Landau, N.R. (2003). Species-specific exclusion of APOBEC3G from HIV-1 virions by Vif. Cell *114*, 21–31.

Marin, M., Rose, K.M., Kozak, S.L., and Kabat, D. (2003). HIV-1 Vif protein binds the editing enzyme APOBEC3G and induces its degradation. Nat. Med. *9*, 1398–1403.

Mehle, A., Goncalves, J., Santa-Marta, M., McPike, M., and Gabuzda, D. (2004). Phosphorylation of a novel SOCS-box regulates assembly of the HIV-1 Vif-Cul5 complex that promotes APOBEC3G degradation. Genes Dev. *18*, 2861–2866.

Münk, C., Beck, T., Zielonka, J., Hotz-Wagenblatt, A., Chareza, S., Battenberg, M., Thielebein, J., Cichutek, K., Bravo, I.G., O'Brien, S.J., et al. (2008). Functions, structure, and read-through alternative splicing of feline APOBEC3 genes. Genome Biol. *9*, R48.

Münk, C., Jensen, B.E., Zielonka, J., Häussinger, D., and Kamp, C. (2012a). Running loose or getting lost: how HIV-1 counters and capitalizes on APOBEC3-induced mutagenesis through its Vif protein. Viruses *4*, 3132–3161.

Münk, C., Willemsen, A., and Bravo, I.G. (2012b). An ancient history of gene duplications, fusions and losses in the evolution of APOBEC3 mutators in mammals. BMC. Evol. Biol *12*, 71.

Navarro, F., Bollman, B., Chen, H., König, R., Yu, Q., Chiles, K., and Landau, N.R. (2005). Complementary function of the two catalytic domains of APOBEC3G. Virology *333*, 374–386.

Niewiadomska, A.M., Tian, C., Tan, L., Wang, T., Sarkis, P.T., and Yu, X.F. (2007). Differential inhibition of long interspersed element 1 by APOBEC3 does not correlate with high-molecular-mass-complex formation or P-body association. J. Virol. *81*, 9577–9583.

Nik-Zainal, S., Alexandrov, L.B., Wedge, D.C., Van, L.P., Greenman, C.D., Raine, K., Jones, D., Hinton, J., Marshall, J., Stebbings, L.A., et al. (2012). Mutational processes molding the genomes of 21 breast cancers. Cell *149*, 979–993.

Nowarski, R. and Kotler, M. (2013). APOBEC3 cytidine deaminases in double-strand DNA break repair and cancer promotion. Cancer Res. *73*, 3494–3498.

Nowarski, R., Britan-Rosich, E., Shiloach, T., and Kotler, M. (2008). Hypermutation by intersegmental transfer of APOBEC3G cytidine deaminase. Nat. Struct. Mol. Biol. *15*, 1059–1066.

Ooms, M., Krikoni, A., Kress, A.K., Simon, V., and Münk, C. (2012). APOBEC3A, APOBEC3B, and APOBEC3H haplotype 2 restrict human T-lymphotropic virus type 1. J. Virol. *86*, 6097–6108.

Perkovic, M., Schmidt, S., Marino, D., Russell, R.A., Stauch, B., Hofmann, H., Kopietz, F., Kloke, B.P., Zielonka, J., Strover, H., et al. (2009). Species-specific inhibition of APOBEC3C by the prototype foamy virus protein bet. J. Biol. Chem. *284*, 5819–5826.

Prochnow, C., Bransteitter, R., Klein, M.G., Goodman, M.F., and Chen, X.S. (2007). The APOBEC-2 crystal structure and functional implications for the deaminase AID. Nature *445*, 447–451.

Rausch, J.W., Chelico, L., Goodman, M.F., and Le Grice, S.F. (2009). Dissecting APOBEC3G substrate specificity by nucleoside analog interference. J. Biol. Chem. *284*, 7047–7058.

Roberts, S.A., Sterling, J., Thompson, C., Harris, S., Mav, D., Shah, R., Klimczak, L.J., Kryukov, G.V., Malc, E., Mieczkowski, P.A., et al. (2012). Clustered mutations in yeast and in human cancers can arise from damaged long single-strand DNA regions. Mol. Cell *46*, 424–435.

Russell, R.A., Wiegand, H.L., Moore, M.D., Schafer, A., McClure, M.O., and Cullen, B.R. (2005). Foamy virus Bet proteins function as novel inhibitors of the APOBEC3 family of innate antiretroviral defense factors. J. Virol. *79*, 8724–8731.

Salter, J.D., Krucinska, J., Raina, J., Smith, H.C., and Wedekind, J.E. (2009). A hydrodynamic analysis of APOBEC3G reveals a monomer-dimer-tetramer self-association that has implications for anti-HIV function. Biochemistry *48*, 10685–10687.

Schumacher, A.J., Hache, G., MacDuff, D.A., Brown, W.L., and Harris, R.S. (2008). The DNA deaminase activity of human APOBEC3G is required for Ty1, MusD, and human immunodeficiency virus type 1 restriction. J. Virol. *82*, 2652–2660.

Shandilya, S.M., Nalam, M.N., Nalivaika, E.A., Gross, P.J., Valesano, J.C., Shindo, K., Li, M., Munson, M., Royer, W.E., Harjes, E., et al. (2010). Crystal structure of the APOBEC3G catalytic domain reveals potential oligomerization interfaces. Structure *18*, 28–38.

Sheehy, A.M., Gaddis, N.C., Choi, J.D., and Malim, M.H. (2002). Isolation of a human gene that inhibits HIV-1 infection and is suppressed by the viral Vif protein. Nature *418*, 646–650.

Sheehy, A.M., Gaddis, N.C., and Malim, M.H. (2003). The antiretroviral enzyme APOBEC3G is degraded by the proteasome in response to HIV-1 Vif. Nat. Med. *9*, 1404–1407.

Shlyakhtenko, L.S., Lushnikov, A.Y., Li, M., Lackey, L., Harris, R.S., and Lyubchenko, Y.L. (2011). Atomic force microscopy studies provide direct evidence for dimerization of the HIV restriction factor APOBEC3G. J. Biol. Chem. *286*, 3387–3395.

Shlyakhtenko, L.S., Lushnikov, A.Y., Miyagi, A., Li, M., Harris, R.S., and Lyubchenko, Y.L. (2012). Nanoscale structure and dynamics of ABOBEC3G complexes with single-stranded DNA. Biochemistry *51*, 6432–6440.

Smith, J.L. and Pathak, V.K. (2010). Identification of specific determinants of human APOBEC3F, APOBEC3C, and APOBEC3DE and African green monkey APOBEC3F that interact with HIV-1 Vif. J. Virol. *84*, 12599–12608.

Song, C., Sutton, L., Johnson, M.E., D'Aquila, R.T., and Donahue, J.P. (2012). Signals in APOBEC3F N-terminal and C-terminal deaminase domains each contribute to encapsidation in HIV-1 virions and are both required for HIV-1 restriction. J. Biol. Chem. *287*, 16965–16974.

Soros, V.B., Yonemoto, W., and Greene, W.C. (2007). Newly synthesized APOBEC3G is incorporated into HIV virions, inhibited by HIV RNA, and subsequently activated by RNase H. PLoS. Pathog. *3*, e15.

Stauch, B., Hofmann, H., Perkovic, M., Weisel, M., Kopietz, F., Cichutek, K., Münk, C., and Schneider, G. (2009). Model structure of APOBEC3C reveals a binding pocket modulating ribonucleic acid interaction required for encapsidation. Proc. Natl. Acad. Sci. USA *106*, 12079–12084.

Stavrou, S., Nitta, T., Kotla, S., Ha, D., Nagashima, K., Rein, A.R., Fan, H., and Ross, S.R. (2013). Murine leukemia virus glycosylated Gag blocks apolipoprotein B editing complex 3 and cytosolic sensor access to the reverse transcription complex. Proc. Natl. Acad. Sci. USA *110*, 9078–9083. doi: 10.1073/pnas.1217399110. [Epub 2013 May 13].

Strebel, K. and Khan, M.A. (2008). APOBEC3G encapsidation into HIV-1 virions: which RNA is it? Retrovirology *5*, 55.

Taylor, B.J., Nik-Zainal, S., Wu, Y.L., Stebbings, L.A., Raine, K., Campbell, P.J., Rada, C., Stratton, M.R., and Neuberger, M.S. (2013). DNA deaminases induce break-associated mutation showers with implication of APOBEC3B and 3A in breast cancer kataegis. Elife *2*, e00534.

Teh, A.H., Kimura, M., Yamamoto, M., Tanaka, N., Yamaguchi, I., and Kumasaka, T. (2006). The 1.48 A resolution crystal structure of the homotetrameric cytidine deaminase from mouse. Biochemistry *45*, 7825–7833.

Wang, T., Zhang, W., Tian, C., Liu, B., Yu, Y., Ding, L., Spearman, P., and Yu, X.F. (2008). Distinct viral determinants for the packaging of human cytidine deaminases APOBEC3G and APOBEC3C. Virology *377*, 71–79.

Wedekind, J.E., Gillilan, R., Janda, A., Krucinska, J., Salter, J.D., Bennett, R.P., Raina, J., and Smith, H.C. (2006). Nanostructures of APOBEC3G support a hierarchical assembly model of high molecular mass ribonucleoprotein particles from dimeric subunits. J. Biol. Chem. *281*, 38122–38126.

Wissing, S., Galloway, N.L., and Greene, W.C. (2010). HIV-1 Vif versus the APOBEC3 cytidine deaminases: an intracellular duel between pathogen and host restriction factors. Mol. Aspects Med. *31*, 383–397.

Xiang, S., Short, S.A., Wolfenden, R., and Carter, C.W., Jr. (1997). The structure of the cytidine deaminase-product complex provides evidence for efficient proton transfer and ground-state destabilization. Biochemistry *36*, 4768–4774.

Yu, X., Yu, Y., Liu, B., Luo, K., Kong, W., Mao, P., and Yu, X.F. (2003). Induction of APOBEC3G ubiquitination and degradation by an HIV-1 Vif-Cul5-SCF complex. Science *302*, 1056–1060.

Yu, Y., Xiao, Z., Ehrlich, E.S., Yu, X., and Yu, X.F. (2004). Selective assembly of HIV-1 Vif-Cul5-ElonginB-ElonginC E3 ubiquitin ligase complex through a novel SOCS box and upstream cysteines. Genes Dev. *18*, 2867–2872.

Zhang, K.L., Mangeat, B., Ortiz, M., Zoete, V., Trono, D., Telenti, A., and Michielin, O. (2007). Model structure of human APOBEC3G. PLoS One. *2*, e378.

Zhang, W., Du, J., Evans, S.L., Yu, Y., and Yu, X.F. (2012). T-cell differentiation factor CBF-β regulates HIV-1 Vif-mediated evasion of host restriction. Nature *481*, 376–379.